Superfilling and the Curvature Enhanced Accelerator Coverage Mechanism

by T. P. Moffat, D. Wheeler, and D. Josell

State-of-the-art manufacturing of semiconductor devices involves the electrodeposition of copper for on-chip wiring of integrated circuits. In the Damascene process, interconnects are fabricated by first patterning trenches and vias in a dielectric medium and then filling by metal electrodeposition over the entire wafer surface. This is followed by a planarization step that leaves an array of wires and interlevel vias embedded in the dielectric matrix. The metallization process, pioneered by IBM, depends on the use of electrolyte additives that affect the local metal deposition rate, thereby resulting in superfilling, or bottom-up void-free filling of trenches and vias.[1,2] An example of this remarkable deposition behavior is given in Fig. 1 where growth as a function of electrodeposition time and feature aspect ratio reveals preferential metal deposition at the bottom of the trenches followed by bump formation above the filled trench.[3]

In the early years of copper Damascene technology an understanding of the superfilling process lagged behind its implementation due to a combination of factors. The first generation of electrolytes contained numerous components and general knowledge of both the chemistry and processing conditions was significantly constrained by proprietary concerns. As a result, early modeling studies focused on traditional leveling theory where the location-dependent growth rate derived from diffusion-limited accumulation and consumption of an inhibiting species on the metal surface.[2,4,5] In these studies it was necessary to empirically modify the area-blockage leveling theory to describe feature filling.[2,4] Despite these modifications, detailed studies of shape evolution and the observation of bump formation above the filled trenches made it clear that superfilling could not be rationalized by traditional transport-limited leveling models.[6-8] At the same time, simplification of electrolyte additive packages to two, (accelerator, suppressor) and three (accelerator, suppressor, leveler) components opened the way for detailed studies of the filling process.[9-11] Subsequently, a curvature enhanced accelerator coverage (CEAC) mechanism was shown to quantitatively describe superconformal film growth that is responsible for bottom-up superfilling of sub-micrometer features in Damascene processing.[12-16]

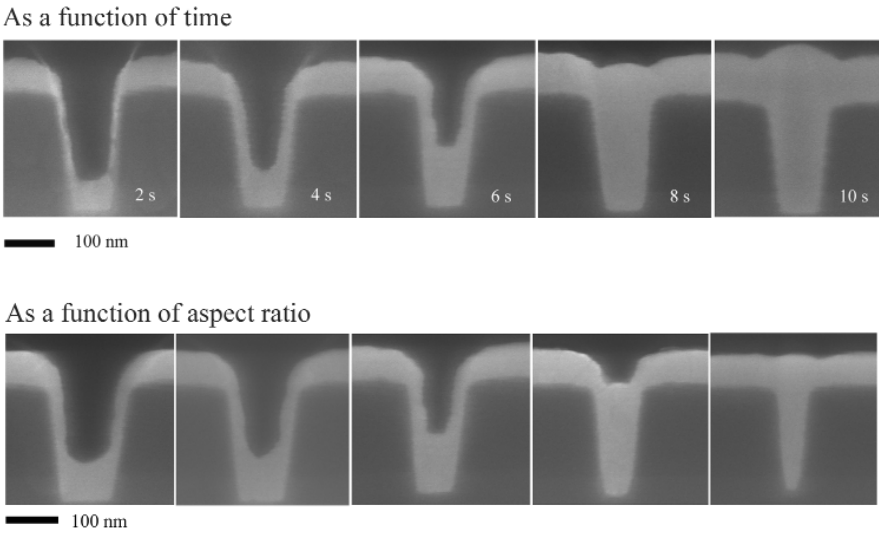

FIG. 1. Bottom-up superfilling of submicrometer trenches by copper deposition from an electrolyte containing PEG-SPS-Cl.[3]

The CEAC Filling Mechanism

The essential idea behind the CEAC mechanism is that (i) the growth velocity is proportional to the local accelerator, or catalyst, surface coverage $\theta_{catalyst}$ and (ii) the catalyst remains segregated at the metal/electrolyte interface during metal deposition. For growth on nonplanar geometries this leads to enrichment of the catalyst on advancing concave surfaces and dilution on convex sections that, in combination, give rise to distinct bottom-up filling of submicrometer features.[12,14-16] The enrichment and dilution processes become increasingly important at smaller (optical) length scales because the change in catalyst coverage for a given deposition rate is proportional to the area change. In terms of the local curvature κ and growth velocity v normal to the surface

$$\frac{d\theta_{catalyst}}{dt} = -\frac{1}{Area}\frac{d(Area)}{dt}\theta_{catalyst} = \kappa v \theta_{catalyst} \qquad [1]$$

A simulation of CEAC-based bottom-up trench filling as applied to copper electrodeposition is shown in Fig. 2. The growth contours are colorized to reflect the local coverage of the catalyst on the growth front. Initially, the catalyst is distributed uniformly along the trench profile, here a fractional surface coverage of 0.054. At first deposition proceeds conformally except for enrichment of the catalyst on the bottom concave corners and the associated formation of 45° inclined surfaces. When the inclined growth fronts meet, further enrichment of catalyst occurs and accelerated growth leads to a flat bottom profile. As the bottom surface advances upward, further

enrichment on the concave sections occurs as catalyst is transferred from eliminated sidewall areas. With the catalyst coverage on the bottom surface approaching saturation, motion of the rapidly advancing bottom surface is accompanied by almost negligible sidewall motion. In contrast, the growth velocity on the convex upper corners is attenuated by dilution of the catalyst that accompanies expansion of the growth front. Similarly, as the bottom surface approaches the upper corners, an inversion of curvature occurs and the growth slows as the highly catalyzed growth front dilates and forms a bump above the feature.

From a more general perspective, the CEAC mechanism represents an extension of the area change effects originally noted in classical dropping mercury electrode studies of surfactant-based charge transfer inhibition.[17] A similar analogy to competitive adsorption on the Langmuir-Blodgett trough is also relevant.[18] Given a surface saturated with two different species, adsorbate-adsorbate interactions must be evaluated. In the limiting case of one species being more strongly bound to the surface, area reduction accompanying motion of a saturated concave surface results in expulsion of the more weakly bound species. In contrast, movement of a convex surface opens up new surface sites for additive adsorption from solution. While specific details may vary, the core principle must remain the correct evaluation of surfactant mass conservation. Interestingly, we recently encountered an earlier assessment of the effects of area change on competitive adsorption at a growing copper electrode in the thesis work of Schulz-Harder.[19-21] The significance of his findings has largely gone unnoticed and it disappeared from the memory of the plating community for more than three decades.[22,23] In light of the substantial industrial investment in copper plating technology, it is probably one of the most unappreciated electroplating works of the 20th century.

A Prototypical Superfilling Electrolyte

The main characteristic of a superfilling electrolyte is competition between inhibitors and accelerators for electrode surface sites.[9-16] The impact on the metal deposition rate is quantified by standard electrochemical methods. A model two- component additive package for copper superfilling contains a mixture of a dilute, *i.e.*, micromolar, sulfonated disulfide accelerator such as SPS [$Na_2(SO_3(CH_2)_3S)_2$] in the presence of a polyether inhibitor, such as PEG (polyethylene glycol, Mw = 3400) that is typically an order of magnitude higher in concentration as indicated in Table I. Effective action of this particular inhibitor and the catalyst requires the presence of halide as a coadsorbate.

Inhibition by PEG-Cl—In a simple cupric sulfate electrolyte, chloride by itself catalyzes the rate-controlling Cu^{2+}/Cu^{+} reaction while PEG alone exerts a negligible influence on the deposition rate.[24-27] In contrast, the combination of PEG-Cl results in nearly two orders of magnitude reduction of the deposition kinetics relative to that for an additive-free solution.[16,26,27] The extent of inhibition is quantified in terms of the effective activity or coverage of a PEG-Cl film that blocks access of Cu^{2+} to the electrode surface.[16,24-27] In what follows, the voltammetric (η-*i*) (Fig. 3a) and chronoamperometric (*i*-*t*) (Fig. 3b) behavior observed with the PEG-Cl electrolyte are used to define the activity (*i.e.*, $\theta_{PEG} = 1$) of the fully inhibited steady-state system and serves as a reference point for subsequent discussion of the effects of SPS adsorption.[16,27]

Catalytic Effect of SPS—SPS additions to the PEG-Cl electrolyte result in disruption of the PEG-based passivating layer and acceleration of the deposition reaction as evident from the hysteretic voltammetric curves shown in Fig. 3a.[16] The metal deposition rate on the negative-going sweep increases with increasing SPS concentration. For the voltammetric conditions employed here, the hysteresis is maximized for an SPS concentration near 2.59 µmol/L. Further additions of SPS result in progressively higher deposition rates on the negative-going potential sweep, while the response on the return scan is effectively saturated. Related potential step experiments yield rising chronoamperometric

Table I. Electrolyte Composition

0.24 mol/L $CuSO_4$
1.8 mol/L H_2SO_4
1.0 mmol/L NaCl
88 µmol/L PEG (3400 Mw)
x µmol/L SPS (*x* = 0 to 500)

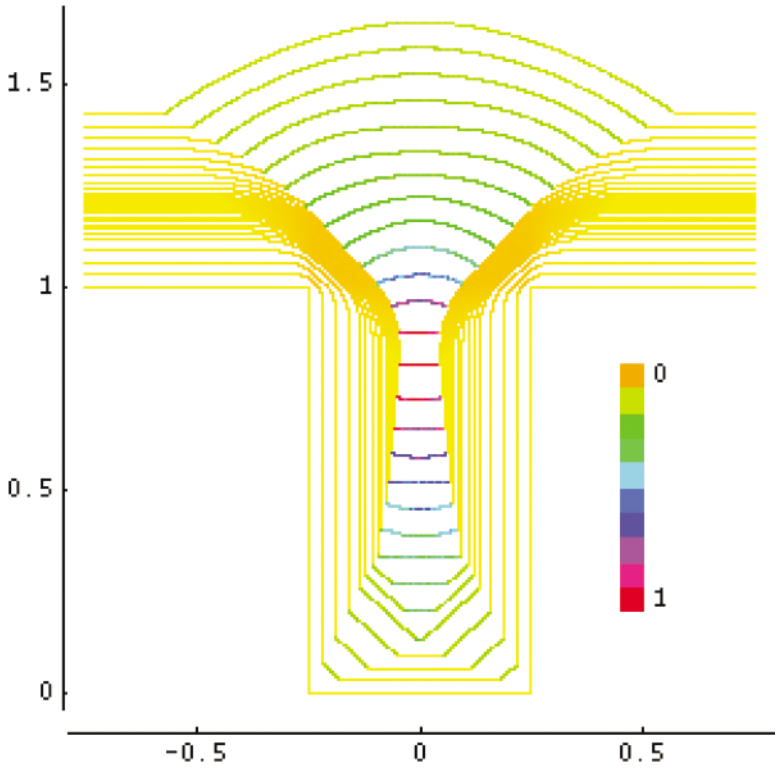

FIG. 2. A simulation of superconformal filling of a SPS-derivatized 0.5 µm wide trench during copper deposition from an acid copper sulfate electrolyte containing PEG-Cl. The contours are colorized to reveal the local fractional coverage of the adsorbed SPS catalyst with the initial value being 0.054.

transients (Fig. 3b) that qualitatively correspond to following a vertical trajectory across the hysteretic *i*-η curves shown in Fig 3a. For a given overpotential the transient rise time decreases monotonically with SPS concentration. The films grown in the presence of SPS are much brighter than those produced in its absence despite the significantly greater cupric ion depletion gradients that accompany growth near the limiting current; the absence of roughening indicates that the hysteretic η-*i* and rising i-t behavior must derive from a change in interfacial chemistry rather than surface area. The data in Fig. 3 can be rationalized in terms of disruption of the rapidly formed PEG-Cl blocking layer by gradual SPS adsorption with the extent of disruption being a monotonic function of the catalyst coverage, θ_{SPS}.[16,27]

The important role of the sulfonate end group is demonstrated by examining the rate of copper deposition on various catalyst-derivatized electrodes in a catalyst-free PEG-Cl electrolyte.[16,27] As shown in Fig. 4, thiols or disulfides with a charged sulfonate terminal group yield significant and sustained catalysis of the metal deposition rate, indicating that they remain on the surface of the deposit and prevent formation of the passivating PEG-Cl film, congruent with the tenets of the CEAC model. In contrast, electrodes derivatized with molecules containing alternative end groups exhibit increased inhibition. In -CH_3 terminated molecules, the increased inhibition is sustained for hundreds of seconds while electrodes modified with -OH or -COOH terminal groups are quickly deactivated, presumably by incorporation of the molecules into the growing solid. The decay rate of the respective current transients may also be used to characterize catalyst consumption kinetics independent of the ambiguities associated with the adsorption process.[16] Integration of a complete transient provides an upper bound estimate of additive incorporation.

Modeling Competitive Adsorption and Its Effect on Copper Deposition

The central role of the SPS-based catalyst is to open channels in the PEG-Cl blocking layer, thereby allowing the Cu^{2+}/Cu^{+} reaction to proceed unhindered, *i.e.*, activation of a blocked electrode. Accelerated copper deposition occurs in the proximity of SPS adsorption sites with neighboring chloride effectively expanding the area catalyzed. Electroanalytical and surface analytical measurements are used to quantitatively examine the potential dependent catalyst adsorption and consumption dynamics. Their potential dependence is most evident from multicycle voltammetry where adsorption that is most rapid at large overpotentials

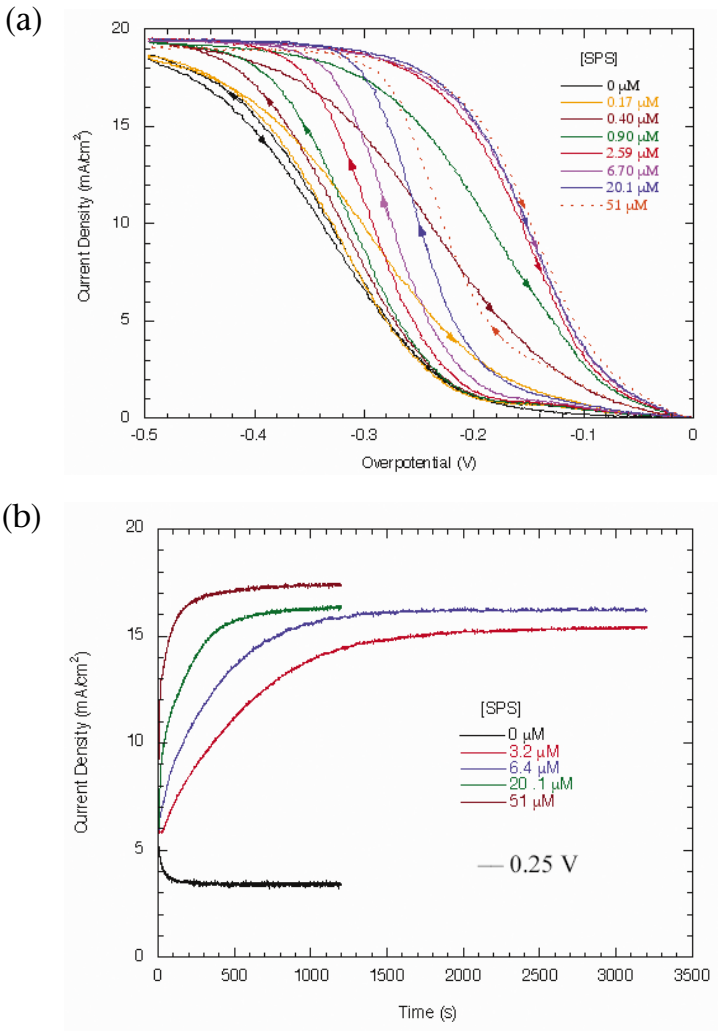

FIG. 3. (a) Hysteretic voltammetry reflects the displacement of inhibiting PEG-Cl species by adsorption of SPS. The bath components are as given in Table I and the scan rate was 1 mV/s for the stationary copper electrode; and (b) Rising chronoamperometry transients characterizing the activation induced by SPS adsorption on stationary PEG-Cl inhibited copper electrodes at –0.25 V.[16]

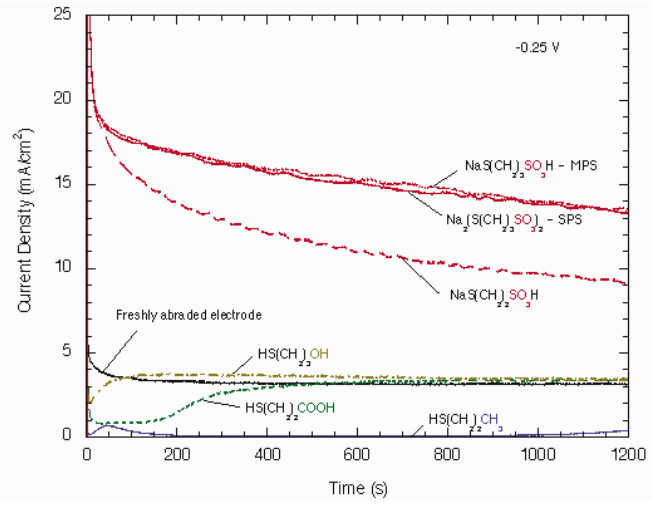

FIG. 4. Chronoamperometric transients establishing the catalytic behavior of sulfonate terminal groups (red) in contrast to the inhibition provided by the (OH, COOH, CH_3) terminal groups.[16]

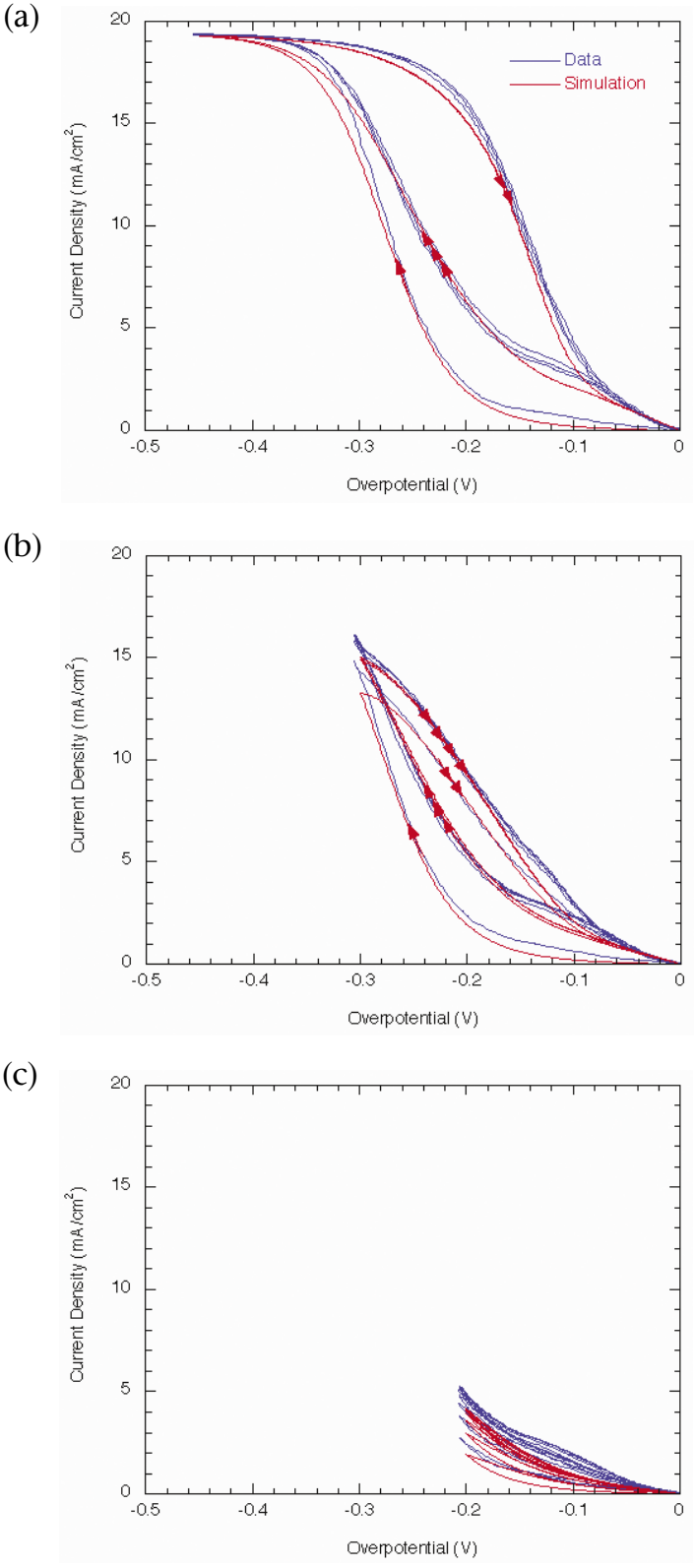

FIG. 5. Variation of the voltmmetric switching potential [(a) –0.45, (b) –0.3, (c) –0.2 V] reveals the strong potential dependence of the catalyst adsorption and consumption. The sweep rate was 1 mV/s and total scan time 2400 s in each experiment.

can be convolved to different degrees with consumption that is most severe at low overpotentials.

Multicycle Voltammetry—As seen in Fig. 5, the second and subsequent negative going sweeps in repetitive potential cycling do not entirely follow the path of the preceding return sweep. The point of departure corresponds to the onset of significant catalyst deactivation.[16,27] The potential dependence of the adsorption rate constant is most clearly revealed by changes in the switching potential. The high metal deposition rate that characterizes the return sweep for a switching potential of -0.45 V is not accessible if the switching potential is smaller than –0.20 V. Voltammograms at intermediate values are consistent with this trend. These results demonstrate that the rate of displacement of the inhibiting PEG-Cl layer by SPS adsorption is an increasing function of overpotential; voltammetric cycling to larger overpotentials permits a larger increase in the catalyst surface coverage that manifests itself as higher currents on the return sweep. Simulations based on competitive PEG vs. SPS adsorption are able to effectively capture the essential characteristics of this system.[16]

Feature Filling: Experiment and Simulation

The most dramatic and unambiguous demonstration of the CEAC mechanism is provided by superfilling of submicrometer features in a two step process that involves derivatization of a patterned copper seed layer with a submonolayer quantity of catalyst, followed by copper plating in a PEG-Cl electrolyte that is free of catalyst. A comparison between the trench filling experiments[16,28] and simulation[16] reveals several distinct and important phenomena that are summarized in Fig. 6.

Experiment—Catalyst derivatization involved a 30 s immersion in a stagnant sulfuric acid solution containing 0.5, 5, 50, 500, or 1000 μmol/L of the catalyst precursor, either the disulfide, SPS, or thiol, MPS. The acceleration of the deposition rate provided by the disulfide (or thiolate) catalyst is evident from the decrease in the feature filling time from ≈ 200 s for specimens derivatized in 0.5 μmol/L SPS to ≈ 40 s for derivatization in 500 mmol/L SPS. For the specimens derivatized in 0.5 μmol/L SPS, deposition proceeds conformally and eventually results in void formation when the rough sidewalls impinge. For the 5, 50, and 500 μmol/L SPS derivatizations, the initial increment of growth is generally conformal except for the onset of accelerated growth at the bottom, concave corners. This yields the V-shaped bottom profile visible in the specimens plated for 70, 40, and 20 s, respectively. Subsequently, catalyst enrichment at the vertex of the V-shaped bottom leads to further acceleration and conversion to a flat bottom

profile. Between 80 and 100 s the 5 μmol/L derivatized specimens exhibit rapid bottom-up filling, the hallmark of the superfilling process. However, by 130 s the sidewalls impinge just before the rapidly advancing trench bottom reaches the top of the feature. The 50 mmol/L specimens exhibit near optimum superfilling behavior with rapid bottom-up filling occurring between 50 and 70 s with negligible sidewall motion. By 70 s the growth front curvature has become convex, and by 100 s a large bump is seen above the trench. For the 500 μmol/L SPS and 1 mmol/L MPS specimens, void formation is clearly evident, this being more severe in the latter case. These experiments provide the strongest evidence that, in accord with the CEAC mechanism, superconformal filling of submicrometer features derives chiefly from the evolution of a submonolayer quantity of a surface-confined catalyst, rather than through transport or chemistry within the electrolyte.

Simulation—The initial catalyst coverages for the respective simulations are indicated in Fig. 6 where the contour lines are colorized to reflect the local catalyst coverage ranging, in order, from orange ($\theta_{SPS} = 0$) through yellow, green, blue, and red ($\theta_{SPS} = 1$). Favorable comparison with experiment is readily apparent.[16] For initial catalyst coverage of 0.00054, deposition is conformal as there is so little catalyst that the effects of geometrical enrichment are negligible. When the initial catalyst coverage is increased to 0.0054 the first indications of superfilling are evident; catalyst enrichment at the bottom corners leads to significant acceleration of the copper deposition rate and formation of inclined growth fronts. Further enrichment accompanies the shape transition from a V-shaped bottom to a flat bottom when the two inclined surfaces meet. The higher catalyst coverage leads to a marked increase in the upward velocity of the bottom surface. Further catalyst enrichment continues through accumulation from the sidewall area being eliminated by the rapid upward motion of the bottom surface. The narrowed bottom surface is predicted to escape the trench barely avoiding impingement of the sidewalls. Increasing the initial catalyst coverage to 0.054 results in robust, near optimal superfilling behavior. As in the previous simulation, the advancing bottom surface accelerates as it collects catalyst from the eliminated sidewall areas, eventually approaching saturation coverage as the bottom surface reaches the top of the trench. From this point on, the expanding surface area associated with the advancing convex section leads to progressive dilution of the local catalyst coverage. In this near optimum case of superfilling the geometrically differentiated surface reactivity predicted by the CEAC model dominates feature filling even in the presence of the substantial metal ion concentration gradient that accompanies the rapid metal deposition.

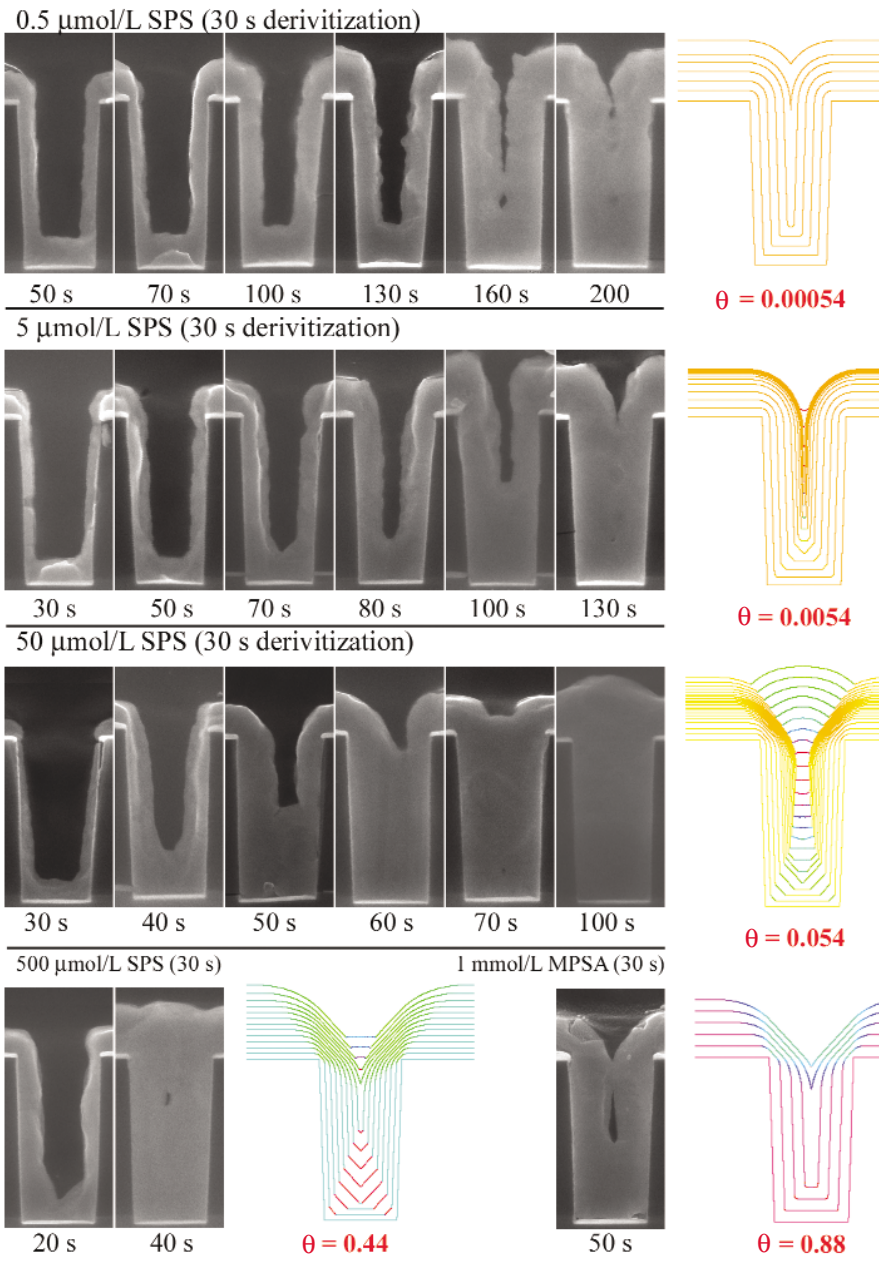

FIG. 6. Superfilling of trenches that were pretreated with catalyst prior to copper plating in a PEG-Cl electrolyte at –0.25 V. The conditions used for electrode derivatization are indicated above the features. Simulations of feature filling for the respective derivatization conditions are shown to the right of the experiments. The contour lines are colorized to reflect the local catalyst coverage. The filling times corresponding to the last simulated growth contour listed in order of increasing adsorbate coverage θ are 177, 113, 85, 39, and 24 s.

Increasing the initial catalyst coverage to 0.44 or 0.88 is predicted to induce a reversion to failure to superfill the trench. In the first case a V-shaped bottom is rapidly established, in agreement with the experiment on the 500 μmol/L - 30 s derivatized SPS electrodes. However, with near-saturation coverage attained on the inclined surfaces, the coverage can rise no further when they impinge, such that no additional acceleration nor the associated flat bottom shape transition can occur at that site.

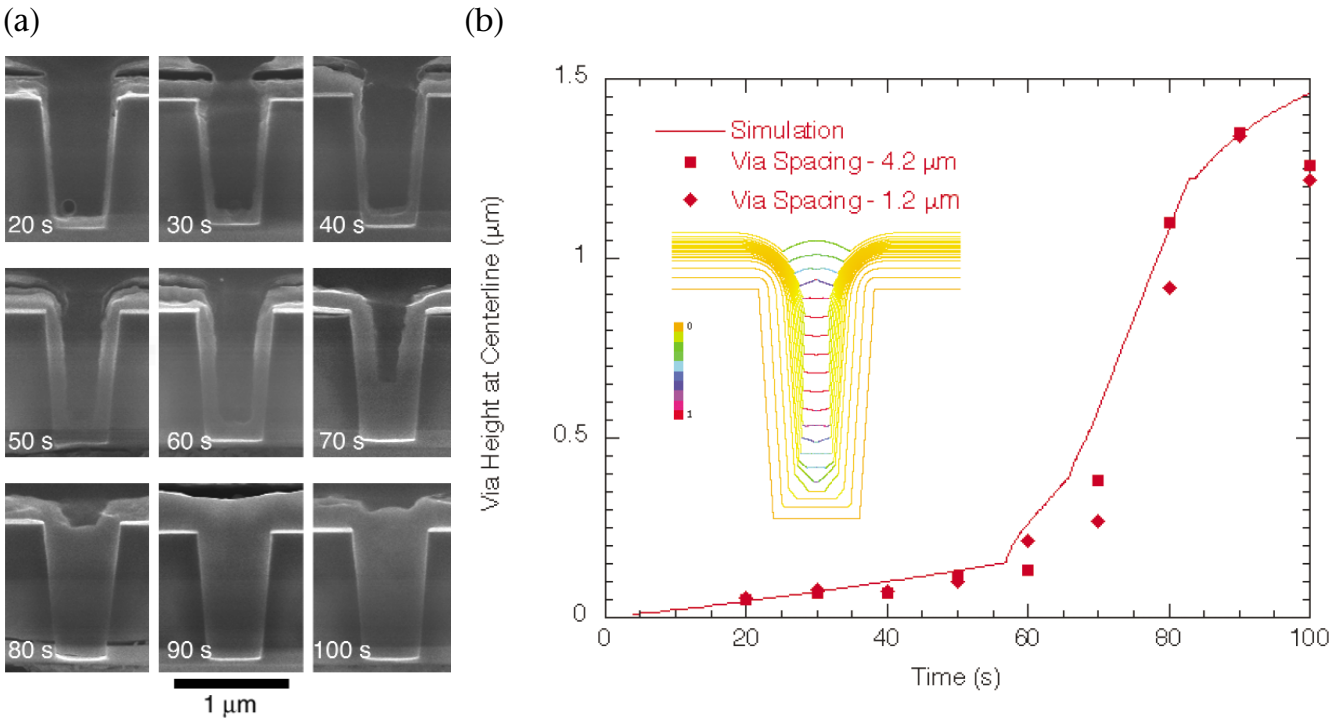

FIG. 7. (a) A time sequence of images showing bottom-up copper superfilling of a via. (b) Tracking the interface midheight position during via filling provides a comparison between the simulation and experiment. The inset shows a θ_{SPS} colorized contour plot of simulated bottom-up film growth.[16]

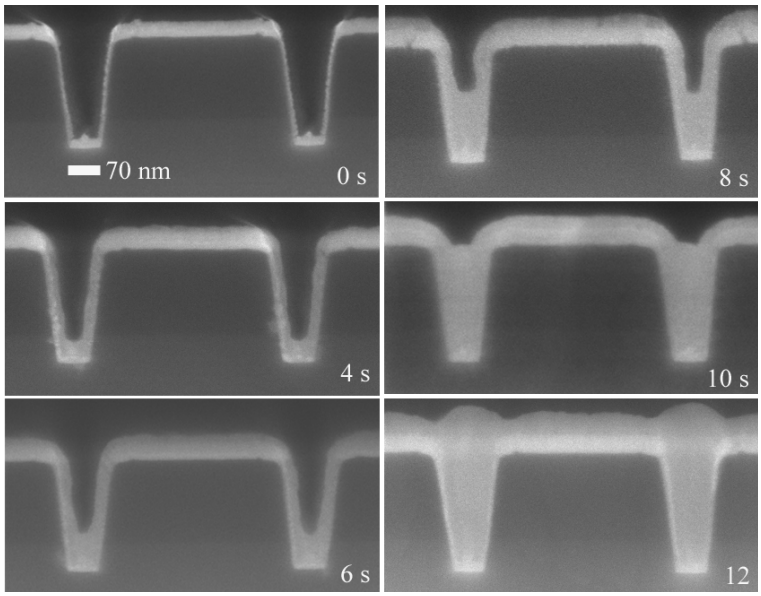

FIG. 8. Seedless superfill is demonstrated by a sequence of images of direct copper deposition on trenches coated with a ruthenium barrier.[3]

With further increases in the differential deposition rate being so constrained, the sidewalls impinge before the bottom surface is able to escape the trench. For initial catalyst coverage of 0.88, the deposition rate is predicted to be effectively saturated at the start of metal deposition with geometrically driven changes in catalyst coverage on the concave surfaces being minimal. Depletion effects are considered only across the hydrodynamic boundary in these simulations. However, for the higher deposition rates associated with higher catalyst coverages, significant depletion of the Cu^{2+} ion occurs within the trench, resulting in faster deposition toward the top of the feature. This leads to an earlier impingement at this location and void formation as observed in two experimental specimens (θ = 0.44 and 0.88) rather than the predicted seams. Such depletion effects have been fully modeled elsewhere.[15]

Via Filling Experiments and Simulations—Deposition in vias, unlike trenches, is a three-dimensional problem by virtue of the nonzero curvature of the cylindrical sidewalls. Cross sections detailing the filling of cylindrical vias with a 4.5° sidewall slope are shown in 10 s increments in Fig. 7.[16] In this experiment the catalyst is adsorbed simultaneously with copper plating in accord with conventional practice. Wafer fragments were immersed in the SPS-PEG-Cl electrolyte, containing 6.4 µmol/L SPS, with a -0.25 V (Cu/Cu^{2+}) growth potential already applied. Growth is essentially conformal for the first 60 s followed by the onset of bottom-up superfilling at ≈70 s. The filling process is summarized by tracking the height of the deposit along the centerline of the via, as a function of deposition time. Favorable agreement with the CEAC simulation is evident and the corresponding simulated growth contours are given in the inset.[16]

Seedless Superfill

Current metallization technology employs three layers, a barrier metal,

typically tantalum, a physical vapor deposited (PVD) copper seed, and electrodeposited copper. As feature sizes continue to shrink, the resistive barrier materials may account for an increasing portion of the cross-sectional area and thus negatively impact electrical performance. These difficulties have driven a search for alternative barrier materials and processes. Ruthenium is a particularly attractive candidate because its electrical and thermal conductivities are approximately twice those of conventional tantalum barriers and ruthenium and copper are immiscible.[29,30] As shown in Fig. 8,[3] direct copper electroplating on PVD ruthenium-seed layers results in rapid coalescence of the copper layer followed by void-free bottom-up superfilling of 70 nm wide trenches in ≈10 s. Such substitution of a noble metal barrier/seed layer for the current Ta/Cu technology promises to offer the combined advantages of process simplification and enhanced performance.

Summary and Outlook

The CEAC mechanism has been shown to explain the bottom-up superfilling used for producing electrodeposited copper interconnects. A quantitative connection between standard electroanalytical measurements on planar electrodes and superfilling of submicrometer features has been developed. This enables inexpensive electroanalytical measurements to be used to screen for potential superfilling electrolytes and offers new insights to process control measurements.[31-33] The CEAC mechanism also provides a natural explanation for brightening because the impact of area change on adsorbate coverage for a fixed increment of growth scales inversely with feature size making it naturally relevant for the length scales associated with optical scattering.[34-35] Finally, the generality of the CEAC has been established by the successful development of superfilling silver[36-37] and gold[38] electrodeposition and copper chemical vapor deposition[39] processes for the filling of submicrometer features. This process technology is likely to also be important to 3D integration of circuits by interchip vias, as well as the fabrication of microelectromechanical systems (MEMS) devices, and other evolving technologies and materials.[40] ■

References

1. P. C. Andricacos, *Electrochem. Soc. Interface*, **8**(1), 32 (1999).
2. P. C. Andricacos, C. Uzoh, J. O. Dukovic, J. Horkans, and H. Deligianni, *IBM J. Res. Dev.*, **42**, 567 (1998).
3. T. P. Moffat, D. Wheeler, C. Witt, and D.Josell, Unpublished research.
4. H. Deligianni, J. O. Dukovic, P. C. Andricacos, and E.G. Walton, in *Electrochemcial Processing in ULSI Fabrication and Semiconductor/Metal Deposition II,* P. C. Andricacos, J. L. Stickney and G. M. Olezak, Editors, PV 99-9, p. 52, The Electrochemical Society Proceedings Series, Pennington, NJ (2000).
5. A. C. West, *J. Electrochem. Soc.*, **147**, 227 (2000).
6. J. Reid and S. Mayer, in *Advanced Metallization Conference 1999*, M. E. Gross, T. Gessner, N. Kobayashi, and Y. Yasuda, Editors, p. 53, MRS, Warrendale, PA (2000).
7. T. Ritzdorf, D. Fulton, and L. Chen, in *Advanced Metallization Conference 1999,* M. E. Gross, T. Gessner, N. Kobayashi and Y. Yasuda, Editors, p.101, MRS, Warrendale, PA (2000).
8. E. Richard, I. Vervoort, S. H. Brongersma, H. Bender, G. Beyer, R. Palmans, S. Lagrange, and K. Maex, in *Advanced Metallization Conference 1999,* M. E. Gross, T. Gessner, N. Kobayashi, and Y. Yasuda, Editors, p. 149, MRS, Warrendale, PA (2000).
9. T. P. Moffat, J. E. Bonevich, W. H. Huber, A. Stanishevsky, D. R. Kelly, G. R. Stafford, and D. Josell, *J. Electrochem. Soc.*, **147**, 4524 (2000).
10. J. Reid, *Jap. J. Appl. Phys.*, **40**, 4B, 2650 (2001).
11. P. Taephaisitphongse, Y. Cao, and A. C. West, *J. Electrochem. Soc.*, **148**, C492 (2001).
12. T. P. Moffat, D. Wheeler, W. H. Huber, and D. Josell, *Electrochem. Solid-State Lett.*, **4**, C26 (2001).
13. A. C. West, S. Mayer, and J. Reid, *Electrochem. Solid-State Lett.*, **4**, C50 (2001).
14. D. Josell, D. Wheeler, W. H. Huber, J. E. Bonevich, and T. P. Moffat, *J. Electrochem. Soc.*, **148**, C767 (2001).
15. D. Wheeler, D. Josell, and T. P. Moffat, *J. Electrochem. Soc.*, **150**, C203 (2003).
16. T. P. Moffat, D. Wheeler, M. D. Edelstein, and D. Josell, *IBM J. Res Dev.*, **49** (Jan2005).
17. A. J. Bard and L. R. Faulkner, *Electrochemical Methods,* J. Wiley & Sons, Inc., New York (1980).
18. A. W. Adamson, *Physical Chemistry of Surfaces,* J. Wiley & Sons, Inc., New York (1976).
19. J. Schulz-Harder, Dissertation, "Ein neuer Mechanismus des Einflusses von Badzusatzen auf die Stromdichteverteilung bei der Metallabscheidung auf rauhen Kathoden und seine experimentelle Begrundung," Technischen Universitat Berlin, Germany(1971).
20. J. Osterwald and J. Schulz-Harder, *Galvanotechnik*, **66**, 360 (1975).
21. J. Osterwald, *Oberflache-Surface,* **17**, 89 (1976).
22. O. Kardos, *Plating*, **61**, 316 (1974).
23. T. P. Moffat, D. Wheeler, and D. Josell, in *Advances in Electrochemistry and Electrochemical Engineering,* R. Alkire, D. M. Kolb, P. Ross, and J. Lipkowski, Editors, Wiley-VCH, Submitted.
24. M. R.. H. Hill and G. T. Rogers, *J. Electroanal. Chem. Interfacial Electrochem.*, **86**, 179 (1978).
25. M. Yokoi, S. Konishi, and T. Hayashi, *Denki Kagaku oyobi Kogyo Butsuri Kagaku,* **52**, 218 (1984).
26. J. J. Kelly and A. C. West, *J. Electrochem. Soc.*, **145**, 3477 (1998).
27. T. P. Moffat, D. Wheeler, and D. Josell, *J. Electrochem. Soc.*, **151**, C262 (2004) (2003).
28. T. P. Moffat, D. Wheeler, C. Witt, and D. Josell, *Electrochem. Solid-State Lett.,* **5**, C49 (2002).
29. D. Josell, D. Wheeler, C. Witt, and T. P. Moffat, *Electrochem. Solid-State Lett.,* **6**, C143 (2003).
30. M. W. Lane, C. E. Murray, F. R. McFeely, P. M. Vereecken, and R. Rosenberg, *Appl. Phys. Lett.,* **83**, 2330 (2003).
31. W. O. Freitag, C. Ogden, D. Tench, and J. White, *Plating*, **70**, 55 (1983).
32. L. T. Koh, G. Z. You, C. Y. Li, and P. D. Foo, *Microelectron. J.,* **33**, 229 (2002).
33. T. P. Moffat, B. Baker, D. Wheeler, and D. Josell, *Electrochem. Solid-State Lett.,* **6**, *C59* (2003).
34. G. B. McFadden, S. R. Coriell, T. P. Moffat, D. Josell, D. Wheeler, W. Schwarzacher, and J. Mallett, *J. Electrochem. Soc.,* **150**, C591 (2003).
35. D. Wheeler, T. P. Moffat, G. B. McFadden, S. Coriell, and D. Josell, *J. Electrochem. Soc.,* **151**, C538 (2004).
36. B. C. Baker, C. Witt, D. Wheeler, D. Josell, and T. P. Moffat, *Electrochem. Solid-State Lett.,* **6**, C67 (2003) and references cited therein.
37. E. J. Ahn and J. J. Kim, *Electrochem. Solid-State Lett.,* **7**, C118 (2004).
38. D. Josell, C. R. Beauchamp, D. R. Kelley, C. A. Witt, and T. P. Moffat, *Electrochem. Solid-State Lett.,* In press.
39. D. Josell, S. Kim, D. Wheeler, T. P. Moffat, and S. G. Pyo, *J. Electrochem. Soc.,* **150**, C368 (2003) and references cited therein.
40. *Advanced Metallization Conference 2002,* A. J. McKerrow, Y. Shacham-Diamand, S. Zaima, and T. Ohba, Editors, Materials Research Society, Warrendale, PA (2003).

About the Authors

T. P. Moffat *is with the Electrochemical Processing Group in the Metallurgy Division at the National Institute for Standards and technology (NIST). His work focuses on the application of electrochemical methods toward understanding thin-film deposition processes. He can be reached by e-mail at thomas.moffat@nist.gov.*

D. Wheeler *is a member of the Center for Computational and Theoretical Material Science at NIST where he uses numerical methods to solve interesting materials science problems. He can be reached by e-mail at daniel.wheeler@nist.gov.*

D. Josell *works in the Materials Structure and Characterization Group of the Metallurgy Division at NIST. His effort centers on the study of thin-film growth phenomena and its effect on the resulting physical properties. He can be reached by e-mail at daniel.josell@nist.gov.*